Improved mapping of flood affected villages in India: a novel three-stage approach using PolSAR polarization signatures and ensembled dilated CNNs

Gopal Singh Phartiyal, Dharmendra Singh, Hussein Yahia

Improved Mapping of Flood Affected Villages in India: A Novel Three-Stage Approach Using PolSAR Polarization Signatures and Ensembled Dilated CNNs

Gopal Singh Phartiyal[a], Dharmendra Singh[b], Hussein Yahia[c]

[a,b]*Department of Electronics and Communication Engineering*

Indian Institute of Technology Roorkee, Roorkee, Uttarakhand – 247667, India

[c]*GeoStat, INRIA, Bordeaux Sud-Ouest-33405, France*

gphartiyal@ec.iitr.ac.in

ORCID identifier: https://orcid.org/0000-0003-1974-4926

Abstract

During floods, updated and accurate information on affected human settlements helps save lives and reduces time to rescue. Therefore, approaches that can provide reliable information during floods via the use of all-weather and real-time functional technology is highly needful. The study presented here attempts to efficiently and precisely map human settlements in the Indian sub-continent during floods via a three-stage approach which uses PolSAR data. However, the sagregation of human settlements in India even with PolSAR data is challenging because the built-up structures in the villages of rural India are closely packed and are randomly oriented w.r.t. each other. This condition either hinders their segregation or otherwise induces false alarms during extraction. More descriptive land cover characterization features and powerful feature classifiers may address this challenge. The study in this paper proposes a novel approach to efficiently detect and map flood affected villages which utilize polarization signatures from PolSAR imagery, ensemble-of -dilated-convolutions based CNNs, apriori knowledge, and image morphology. The approach broadly involves three stages; –first, built-up area extraction from a PolSAR image, -second, detection of villages in a built-up area image and, -third, identification and mapping of villages that are affected by the flood. In the first stage, an ensemble of varying dilated-convolutions based novel CNN classifier which directly utilizes PolSAR-2 polarization signatures (PSs) in window-mode as features are developed to extract built-up areas. The second stage provides a novel village detection filter based on apriori knowledge and image morphology to detect actual villages and mask out the false objects. Finally, in the third stage, flood affected villages are mapped via a series of morphological operations based degree-of-intersection measure. Experiments are conducted on both; simulated and natural flooded area datasets. Experimental results show 81% detection accuracy and 100% mapping performance of the proposed approach which indicates its potential as an effective flood affected village mapping system.

***Keywords*—** Fully polarimetric SAR, Polarization Signatures, Ensembled-Dilated-Convolutions.

1. Introduction

A significant 65% of the Indian population lives in towns and villages and floods are the most frequent, widespread, and damaging disasters for majority this population (*Flood Affected Area Atlas of India - Satellite Based Study* 2023; Jain and Singh 2023). During floods in Indian villages, monitoring and dissemination of rescue operations becomes both critical and challenging at the same time (Mukherjee 2023). Crucial due to the fact that a large proportion of population lives here and challenging because of resiource constraints in these regions for frequent update on the situation. A very good example of resource constraints on rural India compared to urban cities is the study done by researchers in (Young et al. 2022). The study highlights the difference in the social media resoiurce exploitation for information and rescue updates between major cities like Kochi and Tiruvananthpuram and other rural districts of Kerala.

Therefore, to address this crucial but challebging task, a rapid and reliable monitoring is key to minimize the loss of human lives and property in rural parts of India. An accurate and updated near-real-time information of flood affected rural areas can lead to an efficient disaster mitigation plans.

In terms of technologies for flood affected area monitoringin rural India, satellite imaging is one of the most helpful and reliable technology. This resource is geographicaly and socialy unconstrained i.e same fidelity to cities and villages . Especially, the synthetic aperture radar (SAR) imaging modality has proved to be a very effective and all-weather successful technology for monitoring flood affected areas and planning rescue operations (Martinis et a{Citation}l., 2015), (Giustarini et al., 2013)(Sharma et al., 2008).

In particular, the ability of satellite PolSAR imaging instruments to remotely sense the changes in polarization states which in-turn are introduced by the "interaction" of EM waves with earth surface objects (in this case, land covers).

For example, built-up structures usually show double bounce scattering response. It means that these built-up structures appear bright (high backscattering response) in the "HH" image. Whereas, tall vegetation (e.g. forests) show volume scattering response (bright in in "HV" image), and smooth surfaces such as water show single bounce scattering response.

PolSAR imaging has also proved its popularity, significance and unique effectiveness in flood monitoring and mitigation also (Pradhan et al., 2016)(Schnebele et al., 2014)(Dasgupta A. et al., 2017)(Giustarini et al., 2013)

However, mapping human settlements during floods in India is difficult even with PolSAR imagery. The built-up structures (e.g.: Houses) in these human settlements (especially in villages of rural India), are closely packed and randomly oriented with respect to reach other. Therefore, these villages show volume scattering response along with double bounce scattering response in a PolSAR image. The mixed scattering response from these villages hinders their segregation from tall vegetation in a PolSAR image (Garg and Singh, 2018; Mishra et al., 2017; Phartiyal et al., 2020). Therefore, the detection and mapping of these villages during a flood event is challenging even with PolSAR imagery as there is high risk of false alarms and hence ineffective rescue operations. To address such challenges, raw PolSAR data has been transformed and represented in different bases and forms namely decompositions, factorizations, coherency, covariance etc. in various flood monitoring studies (Dasgupta A. et al., 2017; Dumitru et al., 2015; Manavalan et al., 2013; Silvana and Laura, 2018). The current study

proposes the utilization of PolSAR polarization signatures (PSs) features for the detection and mapping of villages that are affected by flood.

Polarization signature (PS) is a two-dimensional or 2D representation depicting backscatter response from any target at a particular polarization state. Polarization signature or PSs are introduced in (Kennaugh and Sloan, 1952) and has been depicted graphically by many researchers in different perspectives (Bielecka et al., 2014; van Zyl et al., 1987). PSs have been proved useful for characterization of land covers (Jafari et al., 2015)(Phartiyal et al., 2020). A comparison of PSs-based features and decomposition-based features for land cover characterization is presented in (Phartiyal et al., 2020). Their study demonstrates the significance of the utilization of PSs over decomposition-based features for land cover characterization and classification in mixed land cover scenarios. This is motivating since a similar scenario is at hand here and therefore, the current study considers PSs as PolSAR features. Theoretical background on PSs is discussed under section 2.

A lack of studies that directly utilize the PSs is notable although normalized signature correlation mapper (NSCM), a correlation-based measure, and normalized Euclidean distance (NED), a distance-based measure, are the popular PSs-derived features used in various applications (de Carvalho and Meneses, 2000), (Maurya et al., 2016).. This is because of the fact that PSs are two dimensional features and a two-dimensional feature extractor would be more efficient to exploit it. As of today, convolutional deep neural networks (CNNs) are one of the most popular, efficient, and powerful image (two-dimensional) feature extractors. Their unique characteristic of “local connectivity” and “parameter sharing” makes them best tools to extract complex and localized features from images (Yann LeCun et al., 2015). Authors in (Phartiyal et al., 2019) explored the significance of CNNs as PSs feature extractors and indicated to the

potential of PSs and CNN based models in other applications. However, more detailed study is required to this end. Therefore, the current study extensively explores the utilization of CNNs as PS feature extractors in order to map flood affected human settlements with PolSAR imagery. The currrent study also explores the [p;arization signature sub-space via dilated convolutions and aggregates the different convolutions to achieve better performance.

To summarize, this paper presents a novel approach to detect and map villages affected by a flood with the help of PolSAR PSs, CNNs, *apriori* knowledge and image morphology. The novel approach involves three stages. These are;

—*first*, design and development of PSs based novel CNN model for extraction of built-up areas from PolSAR image which contains the flooded region,

—*second*, development of methodology for design of village detection filters based on *apriori* knowledge and image morphology and,

—*third*, development of another methodology for identification, and mapping of flood affected villages using image morphology.

This paper is divided into following sections. The fundamentals of the CNNs and the PSs are discussed in section 2. Section 3 provides detailed information on the materials used which involves study areas and datasets considered, and ancillary information collected for the study. Section 4 discusses the three-stage approach development for mapping flood affected villages. Qualitative and quantitative evaluation of the results is also in this section. At last, section 5 concludes the study.

2. Theoretical Background

Polarization Signatures

Polarization signature (PS) is a peculiar representation of backscattering behaviour of a target, or in the case of current study, a land cover. PSs are a two-dimensional in nature. In a polarization signature representation, the *y*-axis and the *x*-axis represent orientation angle and ellipticity angle respectively and the *z*-axis represent the received backscattered power coefficient (σ°). The tilt or orientation angle (ψ) spans from -90° to 90° whereas the ellipticity angle (χ) spans from -45° to 45° The signatures are computed using equation (1). The ellipticity angle represents to the polarization behaviour (i.e. elliptical, circular or linear polarization). On the other hand, the orientation or tilt angle represents to the polarization states (i.e. either horizontal polarization or vertical polarization (Jong-Sen Lee et al., 1997).

$$\sigma(\chi_l \psi_l \chi_m \psi_m) = \frac{4\pi}{k} \begin{pmatrix} 1 \\ \cos 2\chi_l \cos 2\psi_l \\ \cos 2\chi_l \sin 2\psi_l \\ \sin 2\chi_l \end{pmatrix} (\mathbf{K}) \begin{pmatrix} 1 \\ \cos 2\chi_m \cos 2\psi_m \\ \cos 2\chi_m \sin 2\psi_m \\ \sin 2\chi_m \end{pmatrix} \quad (1)$$

where σ represents backscattering coefficient, suffix *m* and *l* represent received and transmit combinations respectively. Given the polarization characteristics of the receiving antenna ,**K** i.e. the Kennaugh matrix, represents the received power (Antenna Laboratory, 1952). It is alternatively termed as the Stokes scattering operator or the Stokes scattering matrix. Computation of the kennaugh parameters is done similar to (Harold, 2007). Further, *k* is the propagation constant. Two variants of PSs are computed namely co-polarized polarization signatures and cross-polarized polarization signatures.

The co-polarized signature is calculated via a transmit and receive settings of $\psi_l = \psi_m$ and $\chi_l = \chi_m$, whereas the cross-polarized signature is calculated via a transmit and receive settings of $\psi_l = 90^o + \psi_m$, and $\chi_l = -\chi_m$. Figure 1 is the co-polarized PS of a sample of a land cover.

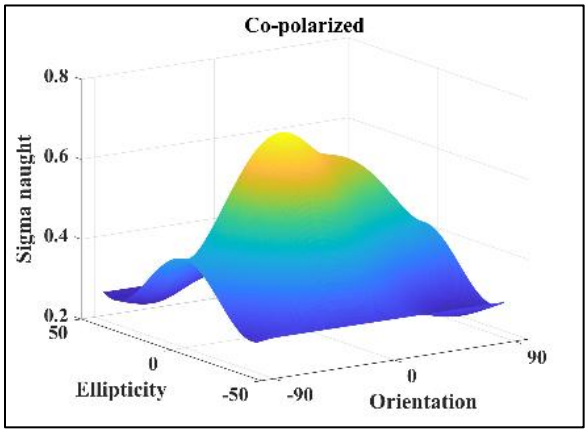

Figure 1 Land cover class sample co-polarized signature.

Convolutional Neural Networks

Convolutional neural networks have become a popular neural network type that utilizes the deep learning technology very well. Fundamental CNN models were proposed in (Ian Goodfellow et al., 2017)(Ciresan et al., 2012) (Fukushima and Miyake, 1982) (LeCun et al., 1998)(Zhang et al., 1991) in the early stages but have quite matured now. For the sake of completeness, the building blocks but not limited to of a conventional CNN are listed here. These are: a convolutional layer with kernel size, activation function, strides and dilation strategy settings, a pooling layer with strides and dilation strategy settings, a dropout layer with dropout fraction, a fully connected layer with node count and activation function, and a loss layer.

Imagine a CNN with *L* layers (including pooling, dropout, or loss), the state vector of the output of the l^{th} convolutional layer is denoted by $\boldsymbol{o}^{l}$, where $l = \{1, 2, 3, \ldots\ldots L\}$ and $\boldsymbol{o}^{0}$ represents the input. Let's say the input is passed onto to a 1D, 2D or 3D convolutional layer based on application. The convolution also intakes a kernel size, filter count, stride and dilation strategy, and activation function. For the sake of reader's interest, a 2D convolution is elucidated here. The convolution plus pooling in the l^{th} layer is represented in equation (2).

$$\mathbf{o}^{l} = pool(g(\mathbf{o}^{l-1} \otimes \mathbf{W}_{l} + \mathbf{b}_{l})) \tag{2}$$

where, $\otimes$ indicates to the convolution operation and *pool* denotes to a spatial aggregation strategy. Weights of the links connecting the $(m-1)^{\text{th}}$ convolutional layer to the m^{th} layer resides in the matrix $\mathbf{W}_{l}$ whereas the vector b_{l} is the bias term. A non-linear pointwise activation function *g*(.) is applied Subsequently. For the selection of dominant features, finally, a pooling layer is placed with a certain window.

If required, any number of convolutional and/or pooling layers queued in any order to constitute a feature extraction architecture that is hierarchical in nature. The last convolution or pooling layer features are reprojected to a one-dimensional feature. Further, this feature is input to a "fully connected" or alternatively termed as "dense" layer which can be perceived as a typical multi perceptron layer. At the end of a CNN network, the final layer is usually a dense layer with either a "linear" activation function (for "regression" scenarios) or a dense layer with a "SoftMax" activation function (for "classification" scenarios) layer. The node count at this layer matches the number of outputs desired.

The weights, $\{\mathbf{W}_1, \mathbf{W}_2, \ldots \mathbf{W}_{\mathrm{L}}\}$ and the biases, $\{\boldsymbol{b}_1, \boldsymbol{b}_2, \ldots \boldsymbol{b}_{\mathrm{L}}\}$ of the CNN represents the parameters of the model. These are learned iteratively and optimized jointly via objective (e.g.

overall accuracy in case of classification) optimization over constraints such as "training" set. Equivalently, models can be realized for 1D or 3D convolution application scenarios.

The aforementioned network in whole, still expresses a single differentiable score function from the 2D input on one end to class scores at the other. The property that 2D CNN architectures make the explicit assumption that the inputs are images. As explored and utilized in the case of PSs in this study which allows encoding certain properties into the architecture. This in turn make the proceeding operations and functions more efficient. CNNs with deep learning have found their application in PolSAR data as well (Zhu et al., 2017).

Materials and Methods

Study Area

For critical analysis, development and evaluation of the proposed three-stage approach, three sites are considered. The first study area is the "Roorkee" city which is situated near the "Rajaji" national park at the foothills of the great Himalayas. This study area spans from $29^{\circ}48'10''N$ latitude, $78^{\circ}4'5''E$ longitude to $29^{\circ}57'4''N$ latitude, $77^{\circ}51'54''E$ longitude. It covers around 361 km^2 of landscape including multiple land covers. This study area is termed as 'Roorkee' study area in this paper. Figure 2(a) shows a true colour Google Earth image of Roorkee. Another study area is the Haridwar city and its neighbouring region. This area extends from $29^{\circ}49'23''N$ latitude, $78^{\circ}10'5''E$ longitude to $29^{\circ}58'23''N$ latitude, $77^{\circ}49'52''E$ longitude. The area amounts to about 270 km^2 of landscape again including multiple land covers such as the river Ganges. This second study area is termed as 'Haridwar' study area in this article. Figure 3(a) shows a true colour Google Earth image of Haridwar. The third study area is considered for validation of the developed approach. This study area is Patna and neighbouring region which were affected

during the ‘Bihar 2016’ floods.

Satellite Data

For the Roorkee and Haridwar study regions, raw single look complex SAR data acquired by the JAXA’s PALSAR-2 L-band fully polarimetric SAR instrument onboard the ALOS-2 satellite on March 13, 2015 is considered. The raw “single look complex” PolSAR data is multilooked, speckle filtered, calibrated, and terrain corrected in that order to obtain backscattering (σ°) coefficients (Phartiyal et al., 2017). Speckle filtering with “Gamma MAP” polarimetric filter is performed analogous to (Mishra et al., 2017) with a 3×3 window size. Calibration and terrain correction are performed in method similar to (Phartiyal et al., 2017). Four features namely HH, HV, VH, and VV are achieved. Intuitively, VH and HV are identical and therefore redundant, only HH, VH, and VV are considered further. Figure 2(b) shows a false colour image of the pre-processed Roorkee dataset and Figure 3(b) shows a false colour image of the pre-processed Haridwar dataset. In addition, for the Patna study area, PALSAR-2 PolSAR image acquired on September 3, 2016 is considered as validation data.

Ground Truth

Ground truth is collected on two counts. First, ground truth sample points are collected for classifier training and validation. Bare soil (BS), built-up, tall vegetation (TV), short vegetation (SV), and water are the five land cover classes considered. On the basis of visual inspection, ground truth class sample points are measured directly on the terrain. A total of 1200 data points are collected separately for two i.e. Roorkee, and Haridwar study areas. More details of the ground truth survey are shown in Table 1.

Second, the total number of villages (a common term opted here to represent all types of human settlements in the study region) in each study area are counted for validation of the proposed approach. Table 1 also lists the actual number of villages in the Roorkee and Haridwar study areas. Further, Figure 4 highlights the villages in the Roorkee and Haridwar study regions captured from Google Earth imagery. Any village in the rural parts of India consists of a minimum of 30 houses and is spread over a minimum area of 5000 m^2. These physical dimensions help in detection of villages in a PolSAR image

It is important to note here that in this paper; different terminologies have been used at different stages to represent different versions of built-up areas. Basic terminologies are defined here.

- Built-up structure: Man-made structures.
- Built-up area: A collection of built-up structures.
- Village or town: Built-up area larger than a predefined size.
- Object: A connected group of image pixels.
- Detected villages: Villages that have been successfully detected
- Flooded villages: Villages that are affected by flood

These terminologies help to better understand the different stages of the study.

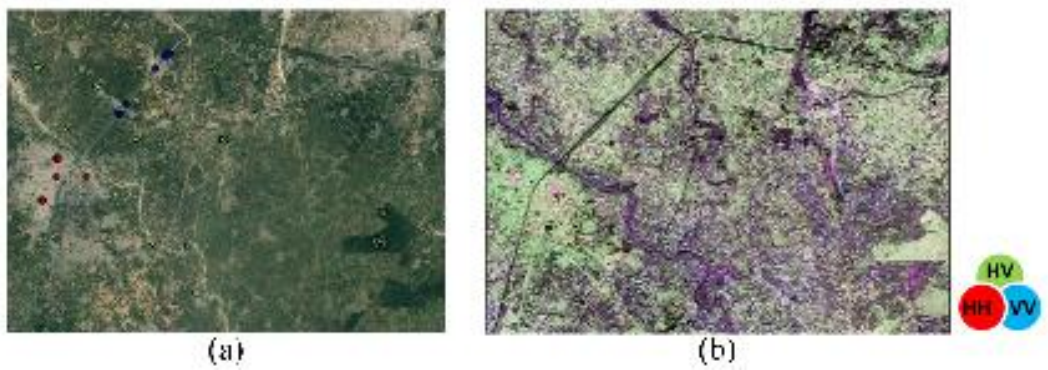

Figure 2. (a): Imagery of the Roorkee collected from Google Earth with major land cover classes marked. (b): FCC of the pre-processed March 13, 2015 PolSAR data.

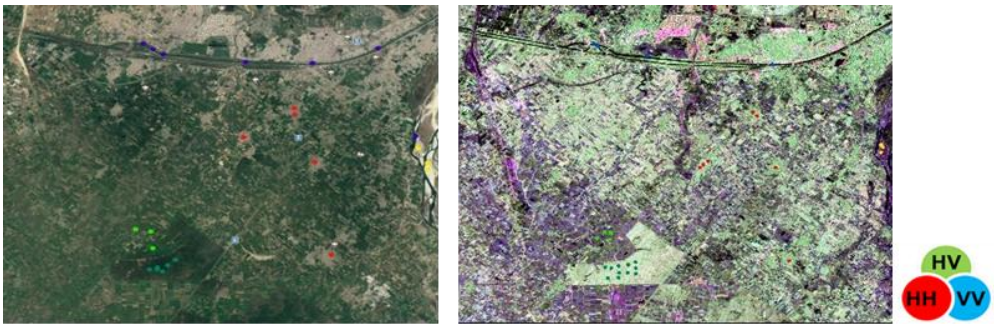

(a) (b)

Figure 3. (a): Imagery of the Haridwar collected from Google Earth with major land cover classes marked. (b): FCC of the pre-processed March 13, 2015 PolSAR data.

Table 1 Ground survey details. TV = Tall Vegetation, *BS =Bare SOIL, SV = Short Vegetation, BU= Built-Up.

LC Class	Roorkee		Haridwar	
	Training	Testing	Training	Testing
Bare Soil (BS)	201	39	201	39
Tall Veg (TV)	201	39	201	39
Short Veg (SV)	201	39	201	39
Built-Up (BU)	201	39	201	39
Water	201	39	201	39
Total	1005	195	1005	195
Total number of villages in Roorkee region	93			
Total number of villages in Haridwar region	60			

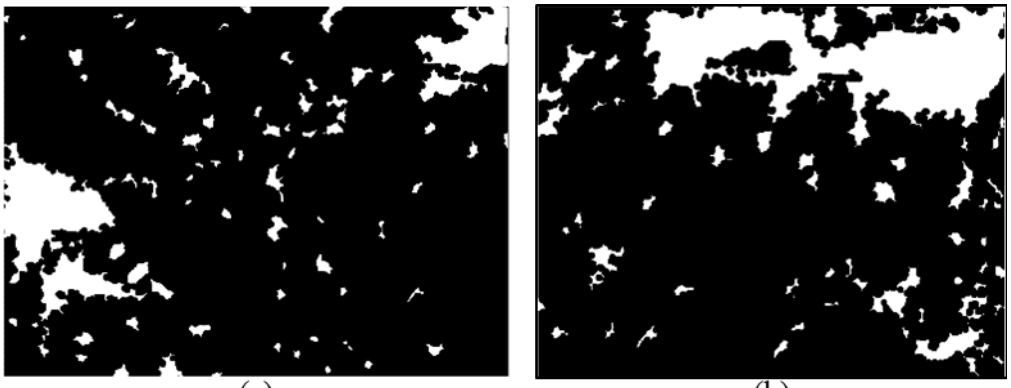

(a) (b)

Figure 4. Areas highlighted in white are villages in the (a) Roorkee and, (b) Haridwar study area.

Approach, Results, and Discussion

This section discusses the development of the proposed novel approach to detect, identify, and map flood affected villages in a PolSAR image. The overall approach is divided into three stages.

In the first stage, design and development of a PSs based CNN model for extraction of built-up areas from PolSAR image is done. This stage is discussed in sections 4.1 and 4.2. Model performance evaluation and comparisons are also discussed in section 4.2.

In second stage, development of a novel methodology, for designing "village detection filters" based on *apriori* knowledge and image morphology, is discussed. These filters help in detection of villages in a 'built-up' class image extracted from classification image (stage-1) and also help suppress false alarms. Section 4.3.1 covers the development of this methodology. Evaluation of the detection performance of this methodology is also covered in section 4.3.1.

Finally, in the third stage, development of methodology, for identification and mapping of villages that are affected by flood and masking out villages that are not, is discussed. This methodology exploits the phenomena of 'enclosed' that happens when a village is surrounded by water (flooded from all sides). Section 4.3.2 discusses the development of this methodology. Evaluation of this methodology is discussed in section 4.3.2. The three methodologies, proposed in the three stages above, sum up to provide a novel 'flood affected village detection and mapping' approach. Flowchart shown in Figure 5 depicts the overall proposed approach.

Land Cover Polarization Signatures

Based to the discussion in section 2.1, both co-polarized signatures and cross-polarized signatures are computed from PolSAR data using equation (1). Co-polarized PS plots for

considered land cover class (averaged over all class samples, refer to Table 1) are shown in Figure 6. Backscatter power response shown in Figure 6 is plotted for orientation angle ψ range (-90° degree to $+90^{\circ}$) degree and ellipticity angle χ range (-45° degree to $+45^{\circ}$) degree and a step size of 5° degree in each direction. This results in a 18×37 two-dimensional feature space. It is evident from figure 6 that PSs of considered land covers are different from each other.

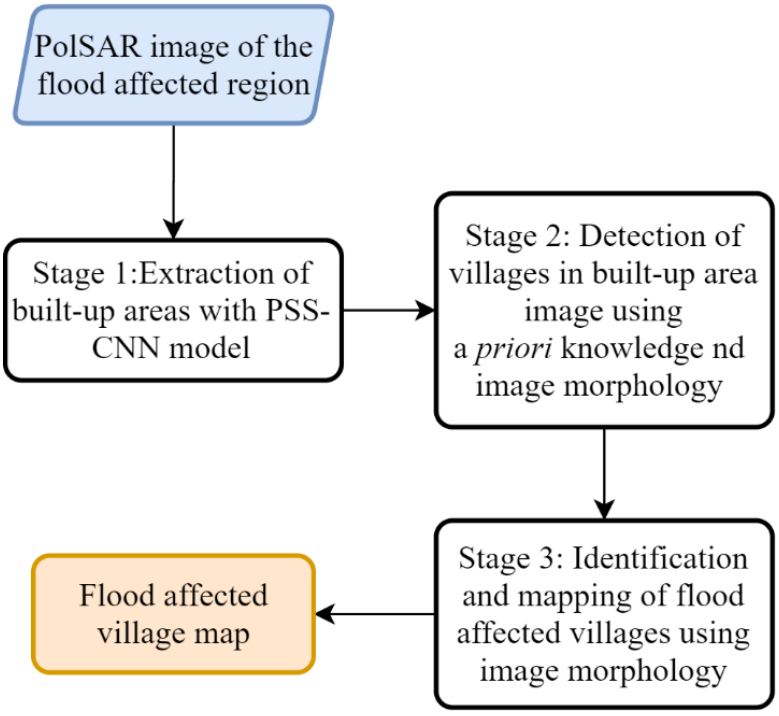

Figure 5.Flowchart of the proposed approach

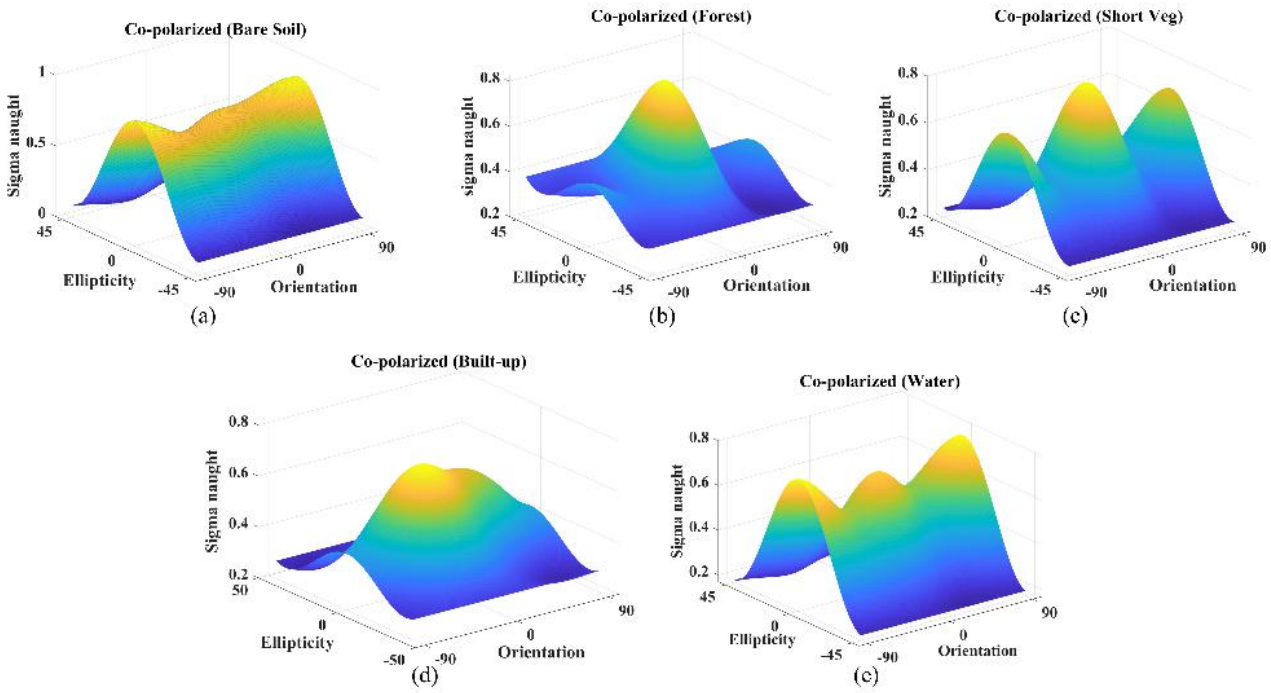

Figure 6 Land cover class co-polarized PSs. (a). Bare Soil, (b). Forest, (c). Ground Vegetation, (d). Built-up, and (e). Water

Stage 1: PolSig-CNN Classification Model for Built-Up Area Extraction

PSs based features have been used for land cover characterization and classification in many studies. Classifiers in (Phartiyal et al., 2017), (Jafari et al., 2015) and (Maurya et al., 2016) used PSs based distance/correlation one-dimensional features which do not consider the two-dimensional neighbourhood during classification and therefore PSs remain under-utilized.

A PSs based CNN classifier is introduced here which explores and extends to more effective utilization of PSs directly with CNNs in order to extract built-up areas from PolSAR images. In this stage, a CNN model is developed to directly utilize PSs as features for built-up area extraction from PolSAR imagery. The proposed CNN model is termed as 'PolSig-CNN' model from here onwards in this paper and, its configuration is provided in Table 2. A two-dimensional spatial window of PSs is used as input. The window-based approach, via averaging,

helps suppresses the random volume scattering responses generated from closely packed built-up structures in built-up areas. This in turn improves the segregation of these built-up areas. A $3*3$ window of neighbouring PSs is considered. This corresponds to a $54*111$ (refer section 4.1) matrix/image as input to the PolSig-CNN model. This $54*111$ input image has two channels i.e. *copol*, and *crosspol*. Therefore, the overall size of the input to the PolSig-CNN is $54*111*2$. The PolSig-CNN used five convolutional layers and three parallel convolutions with different dilation rates. The parallel convolutions with varied dilation rates helps to extract localized polarization feature seb-spaces. This should improve classification performance. The output form these varied convolutions are finally concatenated before connecting to fully connected layers. The number of convolution filters and kernel sizes used in each layer are listed in Table 2. *ReLU* activation function and *Dropout fraction* of 10% is used in each convolutional layer. The dropout regularization strategy is employed to reduce overfitting and achieve better generalization (Srivastava et al., 2014). Further, two *Fully Connected* (FC) layers, first with 50 nodes and second with 10 nodes are used. Both FC layers used the *ReLU* activation function and a *Dropout fraction* of 10%. Finally, a *SoftMax* classification layer with 5 output labels is used. The five output labels are; built-up (BU), water, bare soil (BS), tall vegetation (TV), and short vegetation (SV). A *batch normalization* process is carried out before the convolutions to speed up the training process and to reduce the network sensitivity. Overall, an eight layered PolSig-CNN classification model is realized as shown in Figure 7.

Table 2 Summary of PolSig-CNN model configuration, training and hyperparameter settings. *F = Filters, K = Kernel size, D = Dilation rate

Layer ↓ / Nodes →						Hyperparameters settings
Input	Input image size = $54 \times 111 \times 2$, a 3×3 spatial window with 2 (co- and cross-polarized signatures) Normalization = Batch Normalization					Number of epochs = 200 Learning rate = 0.01 Optimizer = Adam Loss function = Categorical cross entropy
Convolution	**F, K, D***	**Convolution**	**F, K, D***	**Convolution**	**F, K, D***	**Activation, DF**
C-1-1	10, 9×13 , 1×1	C-1-2	10, 5×6 , 9×18	C-1-3	10, 3×3 , 18×37	ReLU, 0.1
C-2-1	10, 9×13 , 1×1	C-2-2	10, 3×3 , 1×1	C-2-3	10, 3×3 , 1×1	
C-3-1	10, 9×13 , 1×1	C-3-2	10, 5×5 , 1×1	C-3-3	10, 5×5 , 1×1	
C-4-1	15, 15×33 , 1×1	C-4-2	15, 5×5 , 1×1	C-4-3	15, 5×5 , 1×1	
C-5-1	15, 15×33 , 1×1	C-5-2	15, 6×15 , 1×1	C-5-3	15, 6×15 , 1×1	
Fully connected	**Filters**					
FC1	50					
FC2	10					
Output layer	5					SoftMax

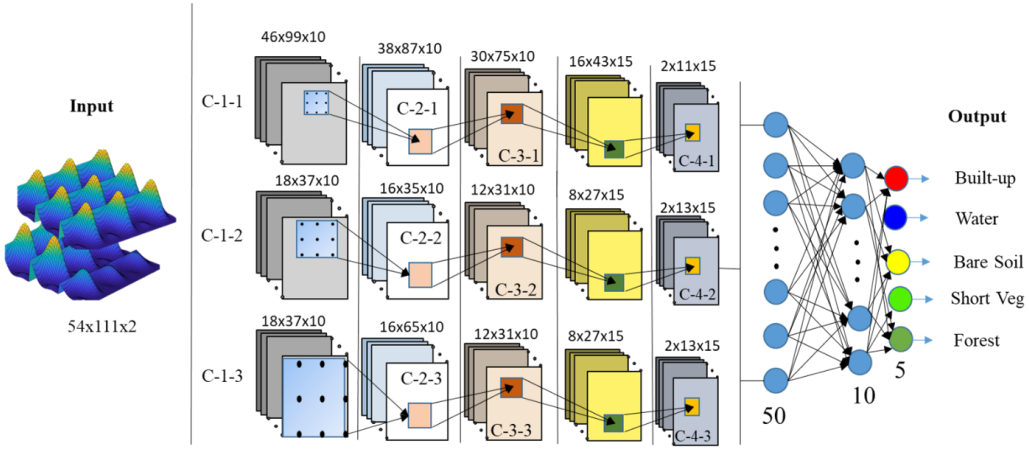

Figure 7 Architecture of the proposed PolSig-CNN model.

The developed PolSig-CNN model is trained on labelled samples collected via ground survey (refer Table 1). The choice of loss function during training is the "*categorical cross entropy"* function. The *learning rate* is set to 0.01 and the number of training *epochs* is set to 200. For network weight optimization, "*Adam"* optimizer is chosen. Model architecture and hyperparameters are set similar for Roorkee and Haridwar datasets for consistency purposes and are listed in Table 2.

Figure 8(a) and figure 8(c) shows the classified image for Roorkee and Haridwar via the PolSig-CNN model. The model's classification performance is compared with two popular feature-classifier pairs that are mostly used with PSs in land cover classification. The first is the normalized signature correlation mapper (NSCM) feature with maximum value classifier and the second is the normalized Euclidean distance (NED) feature with minimum distance classifier. Signature correlation mapper or SCM is a cross correlogram constructed by calculating the cross-correlation between two polarimetric signatures. The SCM obtained from the Pearson correlation coefficient and varies from −1 to 1. The SCM between two signatures p_1 and p_2 is given by equation (3).

$$S(p_1, p_2) = \left(\frac{m\sum_{1}^{m} p_1 p_2 - \sum_{1}^{m} p_1 \sum_{1}^{m} p_2}{\sqrt{\left[m\sum_{1}^{m} {p_1}^2 - \left(\sum_{1}^{m} p_1 \right)^2 \right]} \sqrt{\left[m\sum_{1}^{m} {p_2}^2 - \left(\sum_{1}^{m} p_2 \right)^2 \right]}} \right) \quad (3)$$

where m is the number of polarization states (Jafari et al., 2015)(de Carvalho and Meneses, 2000). NSCM is obtained by normalizing the range of SCM between 0 and 1 using equation (4).

$$S_N = 0.5*(S+1) \quad (4)$$

Euclidean distance (ED) is the distance metric which provides a quantitative measure of the distance between vectors representing the two polarimetric signatures, and it reflects the dissimilarity between the polarimetric signatures (Gower, 1985) (Jafari et al., 2015). The Euclidean distance between two signatures p_1 and p_2 is given by equation (5).

$$D(p_1, p_2) = \sqrt{\sum_{1}^{m} (p_1 - p_2)^2} \quad (5)$$

where *m* is the number of polarization states. Further, NED is the normalized version of ED. Both NSCM and NED have been utilized for land cover characterization (Jafari et al., 2015) and for land cover classification (Maurya et al., 2016).

Figure 8(e) and 8(g) shows classified images using the NSCM as features for Roorkee and Haridwar respectively whereas figure 8(i) and 8(k) shows the classified images using the NED as features for Roorkee and Haridwar respectively. It is evident form Figure 2, Figure 3, and Figure 8(a, c, e, g, i, and k) that the PolSig-CNN classifier outperforms the NSCM-max-correlation classifier and the NED-min-distance classifier on both, the Roorkee, and the Haridwar datasets. Because of the point-wise operability, the limitation of the NED and NSCM classifiers (termed in short) to capture and exploit the two-dimensional neighbourhood relationship of a PS pixel and thereby are not able to efficiently segregate the built-up areas as also discussed in section 1. The developed PolSig-CNN extracts and utilizes the subtle differences in the PSs of built-up and forest and successfully separates the two and hence resolves the issue significantly. It is evident from Figure 8(a) & 8(c) that PolSig-CNN classifier is successful in segregating the two classes. Built-up class is extracted from the PolSig-CNN, NSCM, and NED classified images of and are shown in Figure 8 (b, d, f, h, j and, l). From Figure

8 (b, d, f, h, j and, l), it is evident that the PolSig-CNN is able to segregate the built-up class very efficiently.

Table 3 summarizes the quantitative assessment of classification performance of the PolSig-CNN, NSCM, and NED classifiers for Roorkee and Haridwar datasets. The PolSig-CNN classifier performs land cover classification with good overall accuracies, i.e. 72% for Roorkee and 75.5% for Haridwar dataset. In contrast, the NED performed the classification with 62.5 % and 59.5% overall accuracy and, the NSCM performed the classification with 64% and 66% overall accuracy for the Roorkee and Haridwar dataset respectively. Both NED and NSCM showed low kappa values (refer table 3) whereas the kappa for PolSig-CNN is satisfactory. Furthermore, the PolSig-CNN classifier successfully segregates the built-up class. The built-up class is segregated with 83.7% user and 77.5% producer accuracies for Roorkee and 82.5% user and 82.5% producer accuracies for Haridwar which supports the visual interpretations.

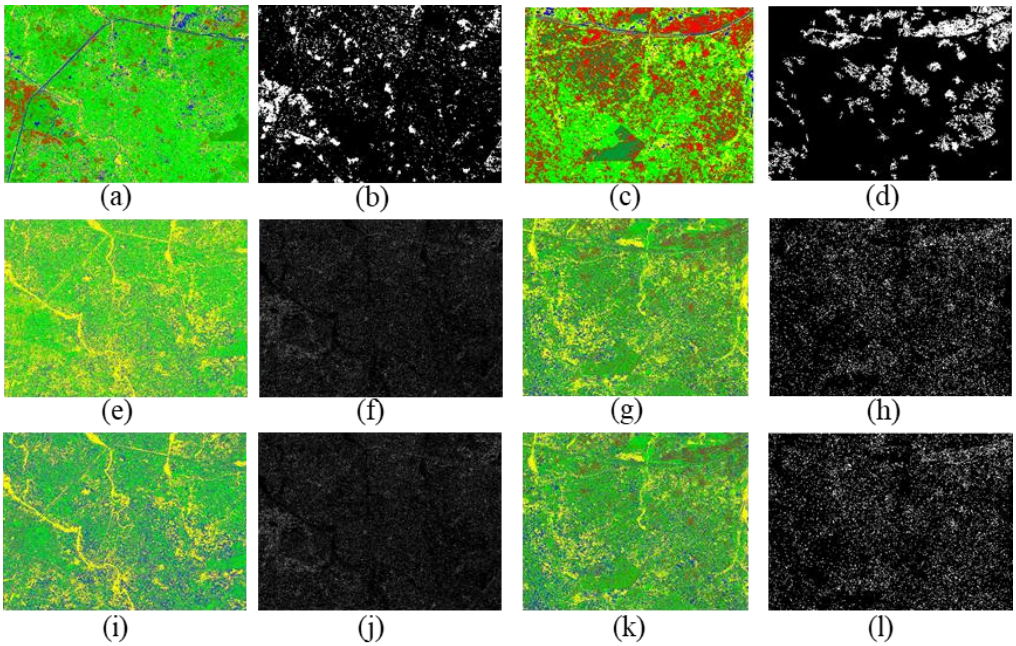

Figure 8. Roorkee classified image obtained using; (a). the PolSig-CNN classifier, (e). the NED classifier and, (i); the NSCM classifier. Areas classified as Built-up in Roorkee dataset using;

(b). the PolSig-CNN classifier, (f). the NED classifier and, (j). the NSCM classifier. Haridwar classified image obtained using; (c). the PolSig-CNN classifier, (g). the NED classifier and, (k); the NSCM classifier. Areas classified as Built-up in Haridwar dataset using; (d). the PolSig-CNN classifier, (h). the NED classifier and, (l). the NSCM classifier.

Table 3 Summary of the classification performance of classifiers for Roorkee and Haridwar datasets. OA = overall accuracy, UA = user accuracy, PA = producer accuracy

Dataset/Study area	**Method**	**OA (%)**	**Kappa**	**Class**	**UA (%)**	**PA (%)**
Roorkee	PolSig-CNN	72.0	0.69	BS	65.91	72.5
				TV	84.21	80
				SV	56.00	70
				BU	83.78	77.5
				Water	77.42	60
	NSCM	64.0	0.57	BS	59.18	72.5
				TV	72.73	60.0
				SV	50.00	70.0
				BU	75.76	62.5
				Water	75.86	55.0
	NED	62.5	0.53	BS	57.45	69.2
				TV	70.59	60.0
				SV	48.21	67.5
				BU	78.13	62.5
				Water	73.33	55.0
Haridwar	PolSig-CNN	75.5	0.72	BS	65.9	72.5
				TV	75.6	77.5
				SV	72.2	65.5
				BU	82.5	82.5
				Water	82.0	80.5
	NSCM	66.0	0.58	BS	65.9	72.5
				TV	72.9	67.5
				SV	48.1	65.0
				BU	75.8	55.0
				Water	77.7	70.0
	NED	59.5	0.52	BS	54.17	66.6
				TV	70.59	60.0
				SV	45.00	67.5
				BU	75.86	55.0
				Water	71.43	50.0

Detection and Mapping of Flood Affected Villages using Apriori Knowledge and Image Morphology

This section presents post classification methodologies based on *apriori* knowledge and image morphology to map the villages affected by flood. Flood affected village maps are obtained using the built-up area image obtained in stage 1. This section covers stage 2 and stage 3 of the proposed approach. The methodology presented under stage 2 detects villages in the built-up area image from section 4.2. This methodology utilizes *apriori* knowledge and image morphology to build village detection filters. Binary morphological image processing is well suited in this case because of the type of outputs produced in stage 1 and the suitability of morphological operations to operate on this data (Zou et al., 2020). These filters detect villages in the built-up area image and significantly remove false alarms or misclassifications. Development of this methodology is discussed under stage 2 in section 4.3.1.

Stage 3 presents a methodology which further identifies and maps villages that are affected by flood and mask out villages that are not affected by flood from the total villages detected in stage 2. This methodology also utilizes image morphology to map flood affected villages. Development of this methodology is discussed in section 4.3.2.

Stage 2: Village Detection

The focus of this stage is to detect villages in the built-up area image obtained in stage 1 (refer section 4.2). Here, at first, the built-up area image ─a binary image─ is cleaned before detection because the image might contain objects (built-up areas) that are close to each other and could be part of same village or, there might be objects with holes in them which is undesirable. These artefacts could lead to inaccurate detection of villages. Therefore, a series of morphological operations are utilized to clean the binary image. The objects or components which are close to

each other, are merged together at first using a morphological image *closing* filter provided in equation (6).

$$\mathbf{I}_{closed} = (\mathbf{I} \oplus \mathbf{S}) \Theta \mathbf{S} \quad (6)$$

where, $\mathbf{I}_{closed}$ is the closed image, **I** is the image on which the morphological closing operation is to be performed, **S** is the structuring element used in the closing operation, and $\oplus$ & θ represents the morphological dilation and erosion operations respectively. The vicinity, within which two objects can be merged together is set via the size of the structuring element parameter. The vicinity is set based on an *apriori* knowledge of the approximate minimum distance between two villages and PolSAR image pixel resolution.

The approximate minimum distance between two villages is set to 200 meters based on ground surveys, geographical metadata. Since, the ALOS PALSAR-2 PolSAR data considered in this study has 6-meter spatial resolution. Therefore, **S** is set as a disc of 15 pixels' diameter (100 meters) and two objects within this distance are merged as one. However, similar relationship can be modelled with other PolSAR imagery. Figure 9(b) depicts the effects of closing operation. It can be observed from figure 9(b) that some objects are merged together.

Next, the holes in the objects in the $\mathbf{I}_{closed}$ image are to be filled. The holes are filled using equation (7).

$$\mathbf{I}_{filled} = \mathbf{I}_{closed} \cup \mathbf{X}_k \quad (7)$$

where, $\mathbf{I}_{\text{filled}}$ is the image with holes filled, $\mathbf{I}_{\text{closed}}$ is the image with holes obtained from equation (6), $\cup$ is the *union* operator, and $\mathbf{X}_k$ is obtained through iterative process governed by equation (8),

$$\mathbf{X}_k = (\mathbf{X}_{k-1} \oplus S) \cap \mathbf{I}_{\text{complement}} \tag{8}$$

where again, $\mathbf{X}_0$ is the $\mathbf{I}_{\text{closed}}$ image, **S** is the connectivity and, $\mathbf{I}_{\text{complement}}$ is the negative of $\mathbf{I}_{\text{closed}}$. Figure 9(c) depicts the result of the hole filling operation.

Finally, an area limit is set to filter out objects that are not villages. The idea is that if any object is to be a village, it must have at least 5000 $m^2$of ground area. The area limit is established based on *apriori* knowledge of the Indian rural human settlements. An area limit (A_L) of 5000 m^2 (140 pixels approx. in case of PALSAR-2 image considered here) is set. Equation (9) demonstrates the process of filtering objects based on its area.

$$(O_k)_{I_{\text{filtered}}} = \begin{cases} 1 & \text{if } (O_K)_{I_{\text{filled}}} > A_L \\ 0 & \text{if } (O_K)_{I_{\text{filled}}} < A_L \end{cases} \text{for } k = 1, 2, ..N \tag{9}$$

where, $(O_k)_{I_{\text{filtered}}}$ is the k^{th} object in the filtered image and $(O_k)_{I_{\text{filled}}}$ is the k^{th} object in the $\mathbf{I}_{\text{filled}}$ image, A_L is the area limit and, N is the total number of objects in $\mathbf{I}_{\text{filled}}$ image. Figure 9(d) depicts output of the area-based filtering. It is observed from Figure 9(d) that many unwanted objects have been removed successfully. The objects remained in the filtered image are successfully detected as villages. In summary, the closing, hole filling, and the area filter

operations in sequence act as a 'village detection filter' which detects villages in a built-up area image and mask out false alarms or misclassifications.

This village detection filter is applied to the built-up area images of the PolSig-CNN, NSCM, and NED. Output images after applying the village detection filter are shown in Figure 10. These output image(s) contain only the successfully *detected villages* and are termed as "DV" image(s) hereafter in this article. The DV images corresponding to the PolSig-CNN, NSCM, and NED classifiers are assessed using reference images. The reference images contain all the villages in the corresponding study areas. The reference images for both Roorkee and Haridwar are provided in section 3.3. Figure 10 shows false colour composites (FCC) of the DV images for Roorkee and Haridwar areas. In Figure 10(a), red colour objects are objects in reference image (actual villages), green colour objects are villages as per the $DV_{PolSig\text{-}CNN}$, and blue colour objects are villages as per the DV_{NED}.

Further, white colour objects are objects which are present in all three images i.e. the reference image, the $DV_{PolSig\text{-}CNN}$ image, and the DV_{NED} image. It means that the object is actually a village and is correctly extracted by both, the PolSig-CNN and the NED classifiers. Yellow colour objects are villages as per the reference and the PolSig-CNN but not as per the NED. Cyan colour objects are villages as per the reference and the NED but not as per the PolSig-CNN. The abundance of yellow colour in Figure 10(a) indicates to the efficient extraction of built-up areas by the PolSig-CNN classifier. Similarly, the $reference\text{-}DV_{PolSig\text{-}CNN}\text{-}DV_{NSCM}$ false colour composite for Roorkee shown in Figure 10(c) evidences the better performance of the proposed PolSig-CNN classifier in built-up area extraction.

However, the $reference\text{-}DV_{PolSig\text{-}CNN}\text{-}DV_{NED}$ and the $reference\text{-}DV_{PolSig\text{-}CNN}\text{-}DV_{NSCM}$ false colour composites for Haridwar in figure 10(b) and figure 10(d) show numerous green colour objects. These objects are falsely detected as villages as per PolSig-CNN and indicate false alarms. A quantitative analysis is therefore required to assess the performance of the classifiers in more detail.

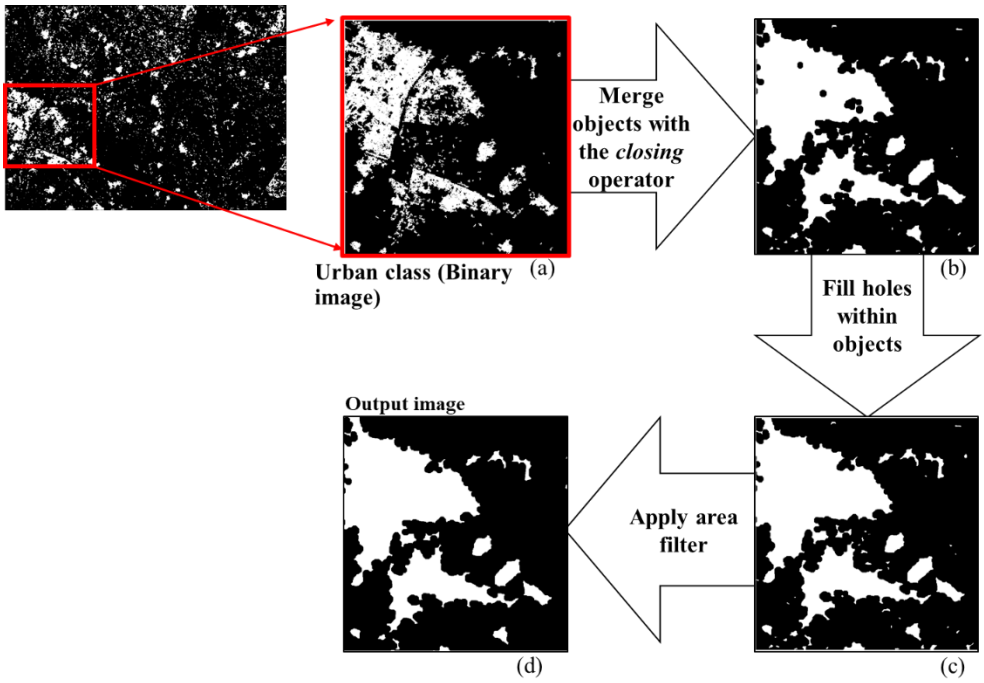

Figure 9 (a). Segment of image shown in figure 6(a). Corresponding segments of: (b). Image after the *closing* operation, (c) Image after the *holes filling* operation and, (d). image after the *filtering* operation

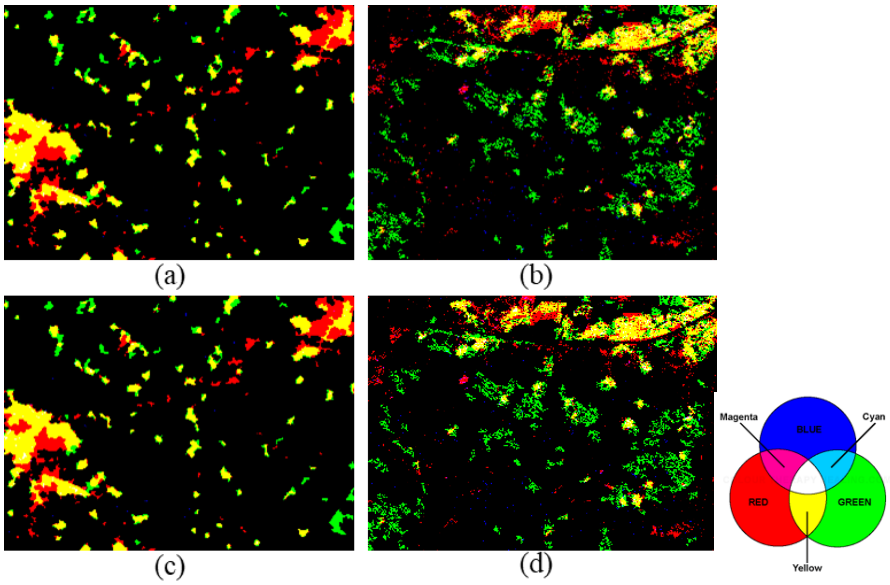

462

463 Figure 10 (a) False colour composites for Roorkee using

464 red = reference, green = $DV_{PolSig\text{-}CNN}$, blue = DV_{NED} colour scheme, (b) False colour composites for

465 Haridwar using red = reference, green = $DV_{PolSig\text{-}CNN}$, blue = DV_{NED} colour scheme, (c) False colour

466 composites for Roorkee using red = reference, green = $DV_{PolSig\text{-}CNN}$, blue = DV_{NSCM} colour scheme,

467 and (d) False colour composites for Haridwar using

468 red = reference, green = $DV_{PolSig\text{-}CNN}$, blue = DV_{NSCM} colour scheme.

469 For quantitative evaluation of the DV images corresponding to the PolSig-CNN, NSCM, and

470 NED classifiers, the following method is considered. At first, a bounding box to mark the extent

471 of each object in both; the reference and the test image, is computed. Then, a bounding box

472 overlap ratio (BBOR) is computed using equation (10) for each pair of objects in the reference

473 and the test image. Test image here represents the 'image under test' which is the DV image

474 from the classifiers.

475
$$(BBOR) = \frac{(\text{Overlap Area})_{(test, reference)}}{\min((\text{Bounding Box Area})_{refrence}, (\text{Bounding Box Area})_{test})} \quad (10)$$

If the BBOR of a particular object pair is above a predefined threshold, then the corresponding object in the test image is counted a successful detection, otherwise not. The threshold is set to 0.5 based on experiment and is set identical for both Roorkee and Haridwar study areas for consistency purpose.

True positives (successfully detected villages), true negatives (villages missed), and false alarms or false positives (objects detected as villages in the test image but are actually not) are computed using equation (11) through (14).

$$\text{True Positive}(TP) = \sum_{i=1}^{m} \text{logical}(IOU_i > \text{threshold}) \tag{11}$$

Where, m is the total number of objects (villages) in the reference image, and

$$\text{logical}(x) = \begin{cases} 1 & \text{if } x > \text{threshold} \\ 0 & \text{if } x < \text{threshold} \end{cases} \tag{12}$$

$$\text{False Negative}(TN) = \text{Total number of villages in reference image} - TP \tag{13}$$

$$\text{False Positive}(FP) = \text{Total number of objects in test image} - TP \tag{14}$$

True positives (TP), False negatives (FN), false positives (FP), and intersection over union (IoU) are computed for Roorkee and Haridwar study areas for PolSig-CNN, NED, and NSCM. Table 4 summarizes the quantities assessment of the DV images of the PolSig-CNN, NED, and NSCM classifiers. The PolSig-CNN successfully extracts 75 (out of 93) villages in the Roorkee study area and 47 (out of 60) villages in the Haridwar study area. Whereas, NED successfully extracts 26 villages in Roorkee and 20 villages in Haridwar and, NSCM successfully extracts 22 villages in Roorkee and 27 villages in Haridwar. The low detection rate

in case of the NED and the NSCM resonates with their low classification accuracies for built-up class (refer table 2).

The false alarms are also high for the NED and the NSCM. The low values of kappa for NED and NSCM (refer table 2) indicate to the high false alarms. The PolSig-CNN offers higher detection rate and low false alarms for both Roorkee and Haridwar study areas.

Table 4 Summary of quantitative assessment of performance of PolSig-CNN, NED, and NSCM.

Dataset	Measures	NED	NSCM	PolSig-CNN
Roorkee	Total number of villages in the study area	93	93	93
	TP (Villages successfully mapped)	26	22	75
	FN (Villages missed)	67	71	18
	FP (or False Alarms)	31	41	1
	IoU	**0.22**	**0.16**	**0.98**
Haridwar	Total number of villages in the study area	60	60	60
	TP (Villages successfully mapped)	20	27	47
	FN (Villages missed)	40	33	13
	FP (or False Alarms)	33	39	5
	IoU	**0.21**	**0.22**	**0.92**

Stage 3: Mapping flood affected villages

Since, any PolSAR image acquired to monitor a flood may include both, flooded and not flooded regions. Therefore, it is important here to identify flood affected villages and mask-out non-flooded villages since the result may impact the planning of a rescue operation. A separate (stage-3) methodology is proposed to achieve this task. The methodology presented in this section encompasses stage 3 of the overall approach.

Intuitively, the villages that are flooded must be completely enclosed by water and villages that are not completely flooded should not be enclosed by water. It means that any village that is completely flooded should appear as 'hole' in the 'water' class image and any village that is not completely affected by flood should not appear as a hole and may have

presence of other class in the vicinity. Based on this interpretation, a criterion is set i.e. if an object in the DV image obtained from section 4.3.1 is a subset of an object in the water class image, then, that object in the DV image is a flooded village otherwise it is a non-flooded village. This criterion separates flooded villages from non-flooded villages.

To realize this criterion, intersection is computed over DV image and the "holes filled" version of water class image. The holes-filled water class image is obtained using equation similar to equation (7). Objects remaining in the intersection image are flooded villages and remaining objects in the DV image is not a completely flooded village. The flowchart of the methodology is depicted in figure 11.

In order to evaluate this methodology, three different 'artificial flood' scenarios are created. The three flood scenarios are shown in figure 12(a-c). In the first scenario as shown in figure 12(a), flood (highlighted in blue) has affected the whole study region whereas in the second and third scenarios, flood has affected some parts of the study region. For experiment, the DV image of Haridwar corresponding to the PolSig-CNN (refer figure 10(b)) is subjected to these three flood scenarios as shown in figure 12(a-c).

In figure 13(a-c), the flood affected villages are marked with yellow colour and the non-flooded villages are marked with red colour. It is evident from figure 13(a-c) that the methodology proposed in this section successfully identifies and maps villages that are completely affected by flood and masks out villages that are not affected by flood. Although, this methodology includes the step 'generation of artificial flood scenarios', however, in real flood situation, this step is skipped and flooded villages can be directly be mapped. The methodology is also evaluated on real flood scenario and results are highlighted in section 4.4.

Overall, two methodologies are proposed in section 4.3. The stage-2 methodology detects villages and removes false alarms and misclassifications in a built-up area image. The stage-3 methodology maps flooded villages and masks out non-flooded villages. These two methodologies in combination with the PolSig-CNN classifier completes the novel 'flood affected village detection and mapping' approach.

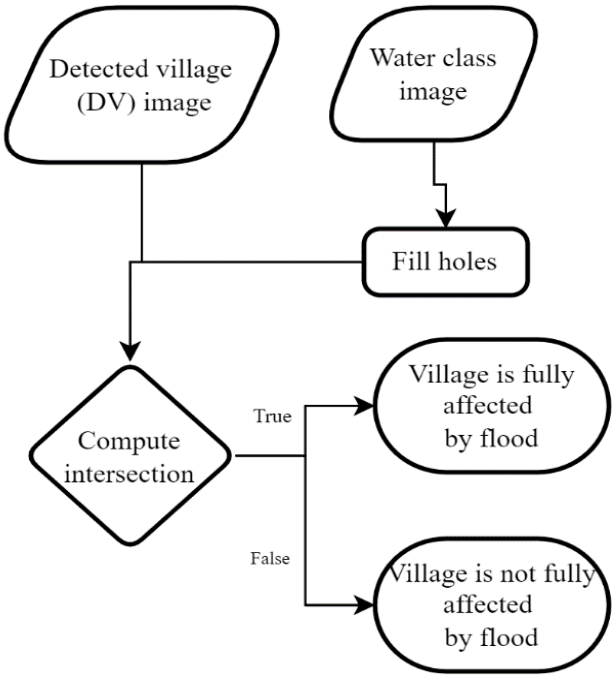

Figure 11 Stage 3 methodology flowchart for flood affected village detection.

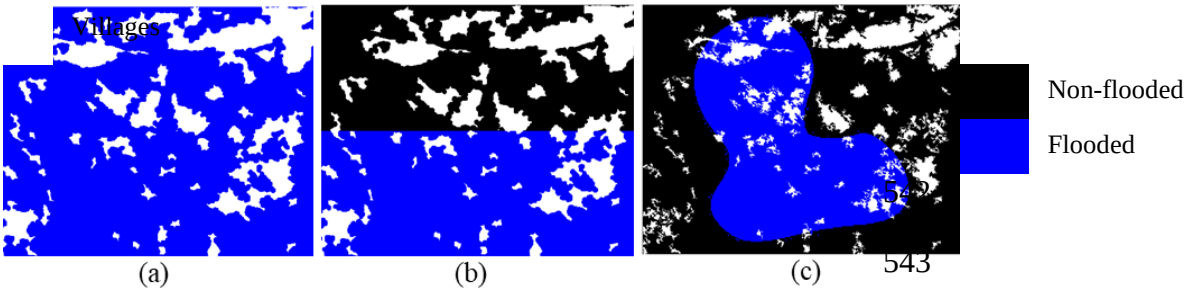

Figure 12 Different artificial flood scenarios; (a) Flood scenario 1, (b) Flood scenario 2 and, (c) Flood scenario 3.

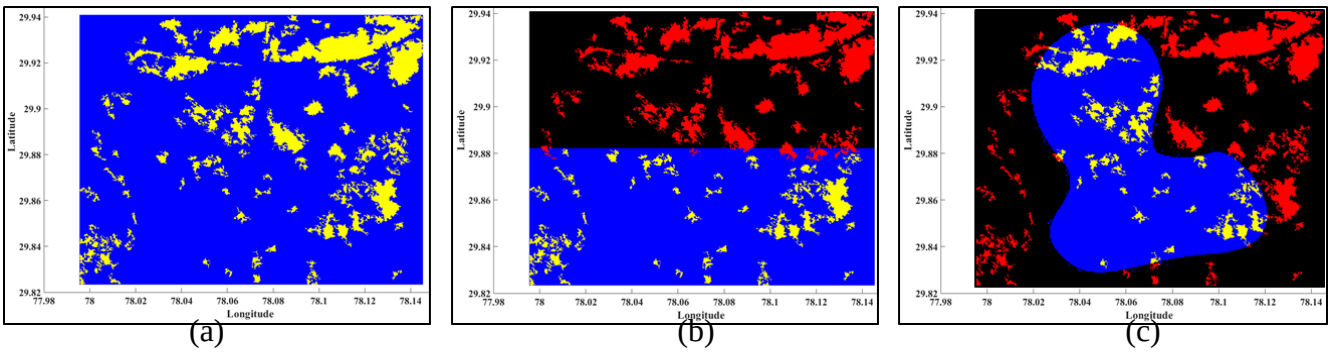

(a) (b) (c)

Figure 13 Flood affected villages (in yellow) and non-flooded villages (in red) under; f(a) Food scenario 1. (b) Flood scenario 2. (c) Flood scenario 3. Colour scheme: yellow = villages affected by flood, red = non-flooded villages and, blue = flooded region.

Validation on real flood scenario

The novel approach proposed in section 4 is validated on real flood PolSAR dataset of Patna, Bihar, India from August 2016. Patna, Bihar sits up at the banks of the river Ganges. The August 2016 Bihar flood affected Patna and neighbouring regions along with other parts of the state. Figure 14(c) shows the FCC of the PALSAR-2 PolSAR data acquired over Patna region on September 03, 2016. The figure clearly highlights the flooded region. The PolSig-CNN classifier used this dataset to create the classification image shown in figure 14(d). The classified image reflects to the flooded situation with presence of 'water' class extensively in the area. Further, 'built-up' class is extracted using stage-2 methodology from the classified image and is shown in figure 14(e). The resulting image is termed as detected-village (DV) image. It is observed that villages in the area are successfully extracted (both flooded and non-flooded). Finally, flood affected villages are mapped using stage-3 methodology and are highlighted with yellow colour in figure 14(f). The final result indicates to the efficiency and effectiveness of the proposed approach in detection and mapping flooded villages using PolSAR data.

Conclusion

This paper presented an efficient approach to map flood affected villages using fully polarimetric SAR imagery. The approach included three stages i.e. *–stage 1*, built-up area extraction, *–stage 2*, village detection and, *-stage 3*, flood affected village mapping.

In the first stage, the approach utilized PALSAR-2 PolSAR polarization signatures (PSs) two-dimensional features and dilated convolutions based CNNs to extract built-up areas. A novel five-class classifier namely PolSig-CNN is developed and trained on 3X3 window PSs class samples, the dilated convolutions based CNN classifier provided improved built-up area extraction because of its ability to capture the two-dimensional neighbourhood relationship of a PS pixel. Quantitative results indicate to approx. 83% classification accuracy for built-up averaged over two different study areas which is promising.

In the second stage, a novel village detection methodology is developed. The methodology detects whether a particular object in the built-up area image, obtained from stage 1, is a village or not using a village detection filter. The detection filter is built on *apriori* knowledge on the minimum average size of rural human settlements in India and image morphology. The detection methodology also significantly removed false alarms and false negatives. A strong detection accuracy of 80% is achieved with this methodology. Qualitative results are also in agreement with the performance.

In the third and final stage, flood affected villages are identified and non-flooded villages are masked out using another image morphology-based methodology. This stage-3 mapping methodology computes a degree-of-intersection between successfully detected villages and flooded area masks and utilizes it for identification of flood affected villages. Experiments are conducted on simulated and real flood datasets and performance of the three-stage approach is

satisfactory. An average detection accuracy of approx. 80% and further, mapping accuracy of 100% is achieved over different study areas. In summary, the three-stage novel approach presented here successfully detects and maps flood affected villages with the help of a PolSAR image. The approach indicates potential to be tested at a real-time.

Acknowledgements

Data: Authors would like to thank JAXA, Japan for providing the ALOS-2 PALSAR-2 dataset. Authors would like to thank IIRS, Dehradun, India for supporting this work. Authors would also like to thank all the lab members of MISTAL, IIT Roorkee for their support.

Declaration of Interest Statement

The authors declare that authors have no conflit of interest.

Data Availability Statement

lab, Availability of the data is subjected to be used exclusively uunder the affiliation of Prof. Dharmendra Singh, ECE Department, IIT Roorkee. Collaborations are invited to use the data for impactful studies.

Word Count: 8562

603

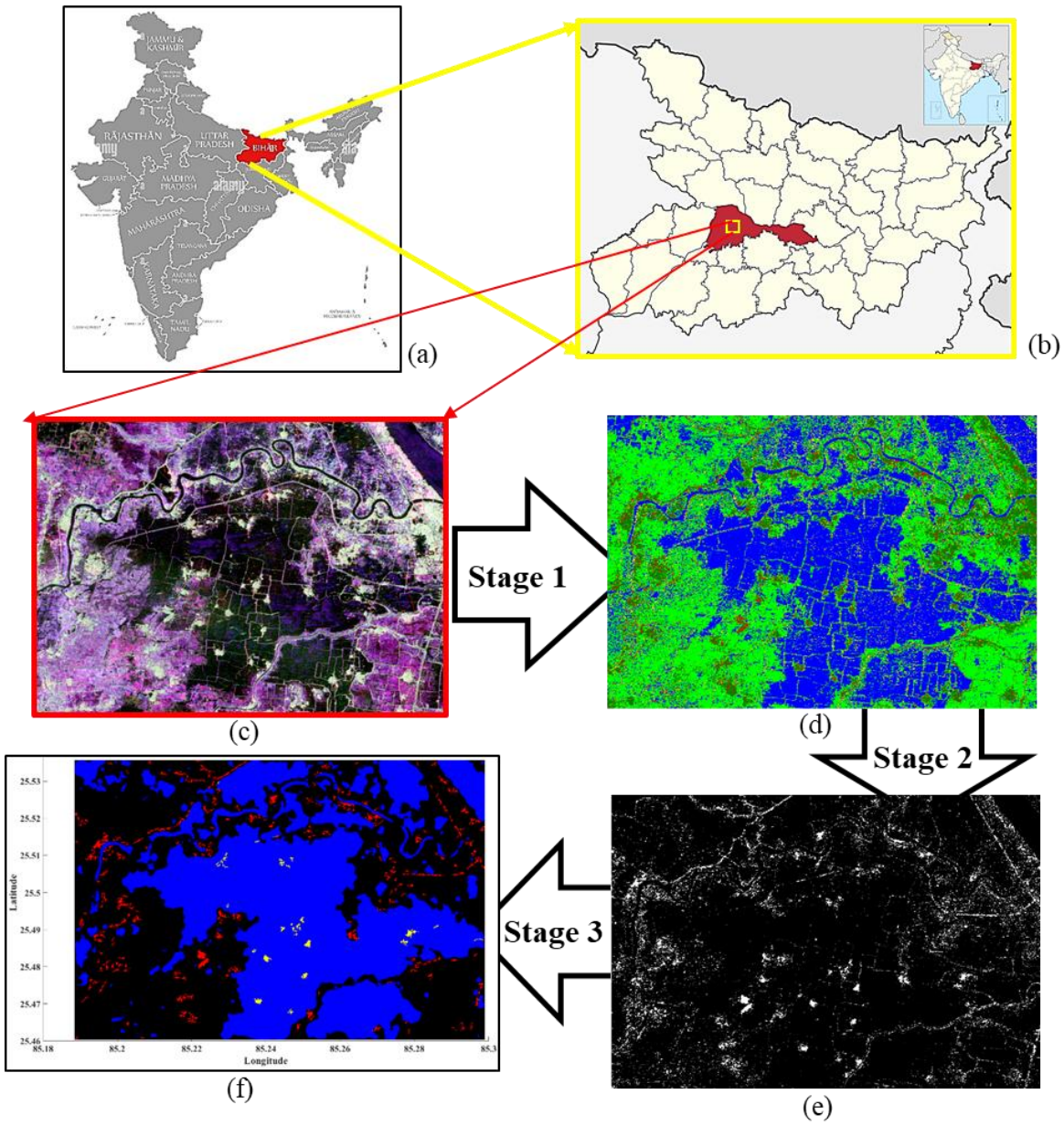

604

605 Figure 14 Validation of the proposed approach. (a) India's state administrative boundaries
606 illustration with Bihar highlighted in red, (b) Bihar's district administrative boundaries
607 illustration with Patna highlighted in red and study area demarcated with yellow box, (c) False
608 color composite (red = HH, green = HV, and blue = VV) PALSAR-2 PolSAR imagery of the
609 validation study area, (d) Classification image using the PolSig-CNN classifier proposed in
610 stage-1, (e) Villages extracted (DV image) using stage-2 methodology, and (f) Flood affected
611 villages (highlighted in yellow) using stage-3 methodology.

References

Antenna Laboratory, D. of E.E., 1952. Effects of Type of Polarization on Echo Characteristics. Columbus, Ohio. https://doi.org/10.1002/nav.3800080206

Bielecka, M., Porzycka-Strzelczyk, S., Strzelczyk, J., 2014. SAR Images Analysis based on Polarimetric Signatures. Applied Soft Computing Journal 23, 259–269. https://doi.org/10.1016/j.asoc.2014.06.013

Ciresan, D., Meier, U., Schmidhuber, J., 2012. Multi-column Deep Neural Networks for Image Classification, in: IEEE Conference on Computer Vision and Pattern Recognition, CVPR. IEEE, Rhode Islan, USA, pp. 3642–3649. https://doi.org/10.1109/CVPR.2012.6248110

Dasgupta A., Grimaldi S., Ramakrishnan R., Walker J. P., 2017. Optimized GLCM-based Texture Features for Improved SAR-based Flood Mapping, in: Geoscience and Remote Sensing Symposium. IEEE, Texas, USA, pp. 3258–3261.

de Carvalho, O.A., Meneses, P.R., 2000. Spectral Correlation Mapper (SCM): An Improvement on the Spectral Angle Mapper (SAM), in: Summaries of the 9th JPL Airborne Earth Science Workshop. JPL Publication, Pasadena, CA, 2000.

Dumitru, C.O., Cui, S., Faur, D., Datcu, M., 2015. Data analytics for rapid mapping: Case study of a flooding event in Germany and the tsunami in Japan using very high resolution SAR images. IEEE J Sel Top Appl Earth Obs Remote Sens 8, 114–129. https://doi.org/10.1109/JSTARS.2014.2320777

Fukushima, K., Miyake, S., 1982. Neocognitron: A Self-Organizing Neural Network Model for a Mechanism of Visual Pattern Recognition, in: Competition and Cooperation in Neural Nets. Springer, Berlin, Heidelberg., pp. 267–285.

Garg, A., Singh, D., 2018. Development of an Efficient Contextual Algorithm for Discrimination of Tall Vegetation and Urban for PALSAR Data. IEEE Transactions on Geoscience and Remote Sensing 56, 3413–3420. https://doi.org/10.1109/TGRS.2018.2799639

Giustarini, L., Hostache, R., Matgen, P., Schumann, G.J.P., Bates, P.D., Mason, D.C., 2013. A Change Detection Approach to Flood Mapping in Urban Areas using TerraSAR-X. IEEE Transactions on Geoscience and Remote Sensing 51, 2417–2430. https://doi.org/10.1109/TGRS.2012.2210901

643 Gower, J.C., 1985. Properties of Euclidean and non-Euclidean Distance Matrices. Linear
644 Algebra Appl 67, 81–97. https://doi.org/10.1016/0024-3795(85)90187-9
645 Harold, M., 2007. The Kennaugh Matrix, in: Remote Sensing with Polarimetric Radar. john
646 Wiley & Sons, New Jersey, pp. 295–298.
647 Ian Goodfellow, Bengio, Y., Courville, A., 2017. Deep learning, Nature Methods.
648 https://doi.org/10.1038/nmeth.3707
649 Jafari, M., Maghsoudi, Y., Zoej, M.J.V., 2015. A New Method for Land Cover
650 Characterization and Classification of Polarimetric SAR Data Using Polarimetric
651 Signatures. IEEE J Sel Top Appl Earth Obs Remote Sens.
652 https://doi.org/10.1109/jstars.2014.2387374
653 Jong-Sen Lee, Mitchell R. Grunes, Wolfgang-Martin Boerner;, 1997. Polarimetric Property
654 Preservation in SAR Speckle Filtering, in: Harold Mott (Ed.), Proc. SPIE 3120,
655 Wideband Interferometric Sensing and Imaging Polarimetry. SPIE, San Diego, pp.
656 1–7. https://doi.org/10.1117/12.300624
657 Kennaugh, E., Sloan, R., 1952. Effects of type of polarization on echo characteristics.
658 Columbus, Ohio.
659 LeCun, Y., Bottou, L., Bengio, Y., Haffner, P., 1998. Gradient-based learning applied to
660 document recognition. Proceedings of the IEEE 86, 2278–2323.
661 https://doi.org/10.1109/5.726791
662 Manavalan, R., Rao, Y.S., Krishna Mohan, B., Venkataraman, G., Chattopadhyay S., 2013.
663 Landuse / Landcover based Flood Area Assessment using L- and C-band SAR Data
664 of Coastal Region of Andhra Pradesh, India, in: Conference Proceedings of 2013
665 Asia-Pacific Conference on Synthetic Aperture Radar (APSAR). IEICE, Tsukuba,
666 Japan, pp. 253–256.
667 Martinis, S., Kersten, J., Twele, A., 2015. A fully Automated TerraSAR-X Based Flood
668 Service. ISPRS Journal of Photogrammetry and Remote Sensing 104, 203–212.
669 https://doi.org/10.1016/j.isprsjprs.2014.07.014
670 Maurya, A.K., Phartiyal, G.S., Singh, D., 2016. A Critical Analysis of Polarimetric
671 Signatures on PALSAR 2 Data for Land Cover Classification, in: Singh, D. (Ed.),
672 IEEE International Conference on Industrial and Information Systems. IEEE,
673 Roorkee, pp. 920–924. https://doi.org/10.1109/ICIINFS.2016.8263070

Mishra, P., Garg, A., Singh, D., 2017. Critical Analysis of Model-Based Incoherent Polarimetric Decomposition Methods and Investigation of Deorientation Effect. IEEE Transactions on Geoscience and Remote Sensing 55, 4868–4877. https://doi.org/10.1109/TGRS.2017.2652060

Phartiyal, G.S., Kumar, K., Singh, D., 2020. An improved land cover classification using polarization signatures for PALSAR 2 data. Advances in Space Research 65, 2622–2635. https://doi.org/10.1016/j.asr.2020.02.028

Phartiyal, G.S., Kumar, K., Singh, D., Singh, K.P., 2017. Optimal Use of Polarimetric Signature on PALSAR-2 Data for Land Cover Classification, in: International Geoscience and Remote Sensing Symposium. pp. 4558–4561. https://doi.org/10.1109/IGARSS.2017.8128016

Phartiyal, G.S., Singh, D., Brodu, N., Yahia, H., 2019. Improved Utilization of Polsar Polarization Signatures Using Convolutional-Deep Neural Nets for Land Cover Classification, in: International Geoscience and Remote Sensing Symposium. IEEE, pp. 5824–5827. https://doi.org/10.1109/IGARSS.2019.8899809

Pradhan, B., Tehrany, M.S., Jebur, M.N., 2016. A New Semiautomated Detection Mapping of Flood Extent from TerraSAR-X Satellite Image Using Rule-Based Classification and Taguchi Optimization Techniques. IEEE Transactions on Geoscience and Remote Sensing 54, 4331–4342. https://doi.org/10.1109/TGRS.2016.2539957

Schnebele, E., Cervone, G., Kumar, S., Waters, N., 2014. Real Time Estimation of the Calgary Floods Using Limited Remote Sensing Data. Water (Basel) 6, 381–398. https://doi.org/10.3390/w6020381

Sharma, R.K., Kumar, B.S., Desai, N.M., Gujraty, V.R., 2008. SAR for Disaster Management. IEEE Aerospace and Electronic Systems 23, 4–9. https://doi.org/10.1109/MAES.2008.4558001

Silvana, G.D., Laura, G., 2018. Adaptive SAR Image Processing Techniques to Support Flood Monitoring from Earth Observation Data, in: Refice, A., D'Addabbo, A., Capolongo, D. (Eds.), Flood Monitoring through Remote Sensing. Springer, Bari, Italy. https://doi.org/10.1007/978-3-319-63959-8

Srivastava, N., Hinton, G., Krizhevsky, A., Sutskever, I., Salakhutdinov, R., 2014. Dropout: A Simple Way to Prevent Neural Networks from Overfitting. Journal of Machine Learning Research 15, 1929–1958.

van Zyl, J.J., Zebker, H.A., Elachi, C., 1987. Imaging radar polarization signatures: Theory and observation. Radio Sci 22, 529–543. https://doi.org/10.1029/RS022i004p00529

Yann LeCun, Yoshua Bengio, Geoffrey Hinton, 2015. Deep learning. Nature 321, 436–444. https://doi.org/10.1038/nature14539

Zhang, W., Hasegawa, A., Itoh, K., Ichioka, Y., 1991. Image Processing of Human Corneal Endothelium Based on a Learning Network. Appl Opt 30, 4211–4217.

Zhu, X.X., Tuia, D., Mou, L., Xia, G.-S., Zhang, L., Xu, F., Fraundorfer, F., 2017. Deep Learning in Remote Sensing: A Comprehensive Review and List of Resources. IEEE Geosci Remote Sens Mag 5, 8-36,. https://doi.org/10.1109/MGRS.2017.2762307

Zou, B., Xu, X., Zhang, L., 2020. Object-Based Classification of PolSAR Images Based on Spatial and Semantic Features. IEEE J Sel Top Appl Earth Obs Remote Sens 13, 609–619. https://doi.org/10.1109/JSTARS.2020.2968966